# The Passivity and Breakdown of Beryllium in Aqueous Solutions

M.A. Hill, D.P. Butt, and R.S. Lillard

Materials Corrosion and Environmental Effects Laboratory
Materials Science and Technology Division
Los Alamos National Laboratory, Los Alamos, New Mexico 87545

## Abstract

The passivity of 98.5% pure beryllium (Be) has been studied as a function of pH. Below pH 2, Be exhibited active dissolution at all applied anodic potentials In solution pH 2-12.5 it is shown that Be exhibited passive anodic behavior at potentials between the open circuit potential and 0.6 V vs. saturated calomel electrode (SCE).. Anodic polarization above 0.6 V SCE in the pH range of 2 - 12.5 lead to an abrupt increase in the passive current density followed by oxygen evolution. This abrupt increase was attributed to a change in the specific resistivity of the passive film above 0.6 V SCE as determined by electrochemical impedance spectroscopy (EIS). EIS experiments were also used to show that the oxide growth rate on Be was 6.4 Å/V over the potential range of 0-4V. At higher anodization potentials the growth rate appeared to be somewhat lower. Breakdown of passivity was studied in chloride and fluoride solutions. In chloride, attack was found to be localized while in fluoride, attack was localized only at concentrations below $10^{-3}$ M. Above fluoride concentrations of $10^{-3}$M, uniform attack was observed. In solutions containing both fluoride and chloride ions, the presence of the fluoride increased the passive current density of beryllium, but had no effect on the pitting potential.

*Key Words* beryllium, pitting, chloride, passivity, electrochemical impedance spectroscopy, anodization, oxide

## Introduction

Beryllium has a hexagonal close packed structure (hcp), high specific heat and thermal conductivity, and high specific strength and stiffness. It is an attractive engineering material for nuclear applications due to its low neutron cross section and for aerospace applications because of its low density (1-5). Disadvantages to using beryllium include respiratory toxicity in particulate form, low fracture toughness, and high cost.

Initial studies of the breakdown of passivity in beryllium focused on those environments expected to be generated in the early "Development Reactors" where beryllium was used as a neutron reflector (6) and are not available in the general literature. In these studies beryllium was exposed to various concentrations of hydrogen peroxide (a water radiolysis product) as a function of solution pH and temperature. At the end of exposure periods, coupons were evaluated for pit density and penetration depth. The effect of coupling beryllium to aluminum and stainless steels on corrosion rate was also investigated. Although beryllium corrosion rates were high in some of the simulated environments, service lifetimes for beryllium reflectors exposed to high purity, low temperature, irradiated water were reported to be good (7).

In general, the literature on other forms of beryllium corrosion is limited. While some polarization studies of beryllium in chloride and sulfate environments have been conducted (8), other investigations have focused on weight loss (9) and visual observation (7) to evaluate susceptibility to corrosion. Levy found that beryllium was susceptible to pitting attack in chloride at its open circuit potential (OCP) and uniform attack (i.e., "...a thick, dark anodic film ...") in $NaNO_3$ solution(8). In addition, it was determined that chromate conversion coatings could be used to mitigate pitting attack in chloride environments at the OCP. Additional studies by Stonehouse and Beaver used humidity cabinet experiments to evaluate the susceptibility of beryllium to corrosion from surface residue deposited during the machining (7).

Other investigations have focused on the corrosion associated with beryllium carbides. One of the primary impurities in historic grades of beryllium was carbon, 0.2 wt.% or more, which results in the formation of second phase particles ($Be_2C$). In the presence of water these carbides react quickly to form BeO ($\Delta G$ = -581 kJ/mol):

$$Be_2C + 2H_2O \rightarrow 2BeO + CH_4 \qquad (1)$$

as discussed by Mueller (10). It may be noted, however, that the relative surface concentration of carbides is low and once the carbide has been consumed no further corrosion of the surface is observed.

The most thorough recent investigation of beryllium passivity as a function of solution pH was conducted by Gulbrandsen et al. (11). In this study phosphoric acid, oxalic acid, phosphate, borate, and carbonate buffer solutions, and sodium hydroxide were used to characterize the passive current density over a pH of 1-15. It was shown that a minimum in passive current density for beryllium occurred near pH 11 and increased logarithmically in more acidic and alkaline solutions. Moreover, it was also observed for any one solution pH, that the passive current density was a function of ionic strength. However, Gulbrandsen did not address the formation of soluble oxalic and phosphoric beryllium complexes that form in some of the solutions used. This may account for their observation of a steady-state passive currents below the thermodynamic limit of pH 2.

This paper is part of a continued effort at the Los Alamos National Laboratory to characterize the corrosion of beryllium in various environments(12, 13, 14). The purpose of the current study is to further our understanding of the passive film associated with beryllium and the breakdown of this film in environments containing chloride and fluoride. Anodization of beryllium and an equivalent circuit model of the passive film are also discussed.

## Experimental Methods

Unless otherwise noted, all samples used in this study were made from Brushwellman S200D grade beryllium discs with a surface area of 1.43 $cm^2$. Electrical leads were connected to the back of the samples with silver paint and epoxy. These leads were encapsulated in glass before mounting the samples in epoxy mounts. Beryllium samples used in potentiodynamic polarization experiments were ground to 400 grit using SiC paper, while beryllium samples used in EIS were ground with successively finer grits of SiC paper followed by polishing on a wheel with diamond paste. The final polish was done using 3 μm diamond paste and performed just prior to testing.

The solutions used for studying passivity as a function of solution pH were: sulfuric acid adjusted to a solution pH of 1 and 2, 0.25 M boric acid (pH=4.6), 0.05M sodium borate / 0.5 M boric acid (pH=7.2), 0.025 M sodium borate / 0.05 M sodium hydroxide (pH=10.7) and sodium hydroxide adjusted to a solution pH of 12.5. Deionized water was used to prepare the test solutions. The pH values reported were measured with a calibrated pH meter. The solutions used for studying the effect of chloride and combined chloride / pH effects were deaerated and consisted of: 0.1 M hydrochloric acid (pH=1), 1 - $10^{-4}$ M NaCl (pH=7), and sodium hydroxide / 0.1 M NaCl (pH=12.5). Deaeration was accomplished with ultra high purity argon for a minimum of six hours prior to running experiments. Chloride containing solutions were mixed with AnalR Grade sodium salts.

The reference electrodes used in these studies were either a mercury / mercurous sulfate (MMSE) electrode which was used with chloride-free solutions or a saturated calomel electrode (SCE) for solutions containing chloride. All potentials are reported vs. SCE. Electrochemical measurements were made using commercially available potentiostats, frequency response analyzers, and software. The open circuit potentials (OCP) of all samples were monitored for one hour prior to beginning experiments to ensure steady state. The scan rate for the polarization curves was 0.1 mV/sec. All anodic curves were run from 100 mV below the OCP to 1-3 V above the open circuit potential and reversed back to open circuit when the current reached a maximum of 1 x $10^{-3}$ amps.

Anodization experiments were conducted in a pH 7.2, 0.5 M boric acid / 0.05 M sodium borate buffer solution at room temperature under ambient aeration. An initial EIS measurement was conducted at the OCP for each sample to determine the thickness of the oxide layer formed at OCP. A 30 minute potentiostatic hold at the given potential was subsequently run. This period was sufficient to allow the current to come to steady state. The sample was then allowed to return to its OCP where subsequent EIS data were collected. The ac voltage signal was applied at frequencies between 10 x$10^3$ Hz and 0.030 Hz and collected at ten points per decade of frequency. Fitting of EIS data was accomplished with complex nonlinear least squares (CNLS) circuit fitting software.

## Results and Discussion

*Characterization of Materials* Powder products are the most commonly used forms of beryllium. Table 1 displays the composition of S200D Be vs. S200F grades of Be, both of which are fabricated from powder materials. The main difference between these grades of Be are the concentrations of BeO, iron, and aluminum (Al). Both grades are manufactured by comminuting vacuum cast ingots followed by grinding or milling to produce powder (15). In this process, a thin oxide layer forms around the Be powder particles resulting in a high BeO content. Figure 1 shows a polarized light micrograph of the S200D Be used in this study. As seen in this figure the grain size of these materials is on the order of 10 - 40 μm which is characteristic of powder products as the BeO particles pin grain boundaries and retard grain growth. The oxide particles in S200D are apparent as small, dark features shown in Figure 1.

*Passivity as a Function of Solution pH* Potentiodynamic polarization curves for Be as a function of pH are shown in Figure 2. Low anodic dissolution rates (less than 1 x $10^{-6}$ A/cm$^2$) were associated with solution pH of 2 to 12.5. Below pH 2, uniform attack of the surface was observed as is evident in the high corrosion current densities ($i_{corr}$) and active anodic current densities measured at this pH. The surface of samples exposed to pH 1 solution were characterized by thick, black deposits over the entire surface. The black deposit was most likely BeO, and has been observed by previous researchers (16). The relationships between passive current density ($i_{pass}$)

and $i_{corr}$ with solution pH are plotted in Figure 3. A minimum in the $i_{pass}$ curve exists in the pH range between 4-11. This differs from Gulbrandsen's result where the minimum in $i_{pass}$ was observed in the vicinity of pH 11(11). The corrosion current density follows a trend similar to the passive current density. However, $i_{corr}$ increases logarithmically below pH 2. Figure 4 shows the Pourbaix diagram for the beryllium-water system at 25°C and for a $Be^{++}$ concentration of $10^{-6}$ and assuming a β crystalline hydroxide film(17). Between pH 4 and 10.7, the formation of the insoluble species $Be(OH)_2$ is thermodynamically favorable. This species, or its hydrate $BeO \cdot H_2O$, likely accounts for the observed passivity of beryllium in this pH range where values of $i_{corr}$ were found to be less than 0.1 $\mu A/cm^2$ and values for $i_{pass}$ were on the order of 0.3-0.9 $\mu A/cm^2$ (Figure 3). While thermodynamically, the formation of soluble $Be^{++}$ is favorable upon anodic polarization in acidic solutions below pH 4 (Figure 4), here uniform attack of the surface was not observed at pH 2 and above. Above a pH of 10.7 the formation of the soluble $Be_2O_3^{--}$ and $BeO_2^{--}$ species is favorable, however, Be passivity was observed at solution pH as high as 12.5.

Also shown in Figure 4 are the OCPs for Be as a function of pH. In deaerated acidic solutions, the OCP was -0.92 V (SCE) and varied by only ± 20 mV during the course of our investigations. In deaerated neutral pH the OCP was -0.99 V (SCE) while in pH 12.5 it was -1.18 V (SCE). These values compare well with those measured by Gulbransdsen(11). Further, the OCP decreased 0.14V per unit increase in pH, compared to a 0.13V per unit increase found by Gulbrandsen(11). To examine the cathodic reaction mechanism at the OCP, cathodic polarization experiments for Be in pH 7 and pH 12.5 solutions under *ambient* aeration were performed. As seen in Figure 5, the OCP of Be in these solutions is approximately and -0.71 and -1.12 V SCE, respectively. These potentials are approximately 50 and 140 mV more negative than reversible hydrogen potential at pH 7 and 12.5. For the pH 7 solution a region of mixed oxygen reduction and hydrogen evolution was observed between the OCP and approximately -1.10 V SCE. Below -1.2 V SCE, hydrogen evolution was observed. For pH 12.5, hydrogen evolution was observed at all potentials below the OCP. The slope of the Tafel region of hydrogen evolution was approximately 160 mV per decade of current at pH 7 as compared to 150 mV per decade of current at a pH of 12.5. At higher cathodic overpotentials, the hydrogen evolution reaction mechanism becomes limited by mass transport. This is apparent in the pH 12.5 curve where the limiting current density is approximately $10^{-2}$ amps/cm$^2$.

Figure 6 shows potentiodynamic polarization curves for Be in pH 7 and 12.5 solutions at more positive potentials than presented in Figure 2. This figure also presents the “return” portion of the polarization curve which scans from more noble potentials to more active potentials. In both pH 7 and 12.5 solutions, abrupt increases in $i_{pass}$ were observed at anodic potentials of approximately 0.60 - 0.83 V and 0.27 - 0.48 V SCE, respectively. These abrupt increases were followed by an apparent seconf $i_{pass}$ which was approximately a factor of 3-10 times higher than the previous values. For the pH 7 solution, the abrupt increase in $i_{pass}$ was approximately 80 mV more positive than the oxygen evolution potential (0.52 V SCE) and in pH 12.5 solution, the abrupt increase occurred approximately 20 mV more positive than the oxygen evolution potential (0.25 V SCE). Moreover, an abrupt decrease in the anodic current densities were observed during the reverse scan indicating that the process was reversible. Although these phenomena are consistent with oxygen evolution, the plateau in the current densities at 0.83 and 0.48 V SCE are inconsistent with oxygen evolution. Moreover, transpassivity[*] was observed for both solutions at approximately 1.8 V SCE as indicated by the logarithmic increase in current density at this potential. Thus oxygen evolution is ruled as a possible mechanism for the observed abrupt increase in $i_{pass}$. Gulbrandsen(11) noted transpassivity above the oxygen evolution potential and concluded that the BeO protective layer may behave as a semiconductor at these potentials. BeO is an n-type semiconductor, characterized by an excess of cations ($Be^{2+}$) which move interstitially through the BeO (19). Mott-Schottky plots were generated at potentials above the abrupt increase in anodic current density in a method similar to Azomi *et al.*(20). However, these results were inconclusive. Further analysis of oxide resistivity as a function of applied potential is presented in the following section of this paper.

---

[*] Here, transpasivity is defined broadly as the potential region more noble than that corresponding to passivity where a small increase in potential is associated with a large increase in current according to Landolt(18). This definition includes metal dissolution, solution oxidation (oxygen evolution), or some combination of both as an explanation for the observed increase in current independent of the reaction mechanism. However this does not include transpassivity as observed for the Cr(III) to Cr(VI) transition, as no oxidation state above Be(II) exists.

*Anodic Oxidation* Typical Bode magnitude and Bode phase plots for beryllium before and after anodic oxidation are shown in Figures 7a and 7b, respectively. As may be expected, the low frequency impedance was greater for the anodized sample. The two minimums observed in the Bode phase data (Figure 7b) are consistent with the two-time-constant equivalent circuit model shown in Figure 8. This model consists of $C_{ox}$, the space charge capacitance of an oxide layer, and $C_{dl}$, the double layer capacitance at the electrode/solution interface, the charge transfer resistance ($R_{ct}$), the oxide resistance ($R_{ox}$), and the ohmic resistance of the solution between the working and reference electrodes ($R_{sol}$). The high frequency time constant was attributed to the oxide and the low frequency time constant to charge transfer. This model is similar to that used by Kolman and Scully to measure oxide thickness as a function of anodic potential on β titanium (21) and by Bohe *et al.* to investigate the semiconducting properties of zinc oxide passive films (22). All EIS data are interpreted in terms of this equivalent circuit model. At all potentials studied $R_{ct}$ was found to be three orders of magnitude greater than $R_{ox}$ (see Table 2).

Oxide thickness as a function of applied potential was calculated using the parameters obtained from circuit fitting and the well known relationship:

$$d_{ox} = \varepsilon\varepsilon_o A/C_{ox} \qquad (2)$$

where $d_{ox}$ is the oxide thickness in cm, $C_{ox}$ is the oxide capacitance obtained from equivalent circuit fitting (see Table 2) in farads, $\varepsilon$ is the dielectric constant, and $\varepsilon_o$ is the permittivity of free space ($8.85 \times 10^{-14}$ farads/cm), and A is the surface area in $cm^2$. The dielectric constant used for beryllium oxide was 6.3 (23). The thickness for the oxide layer formed at the OCP was determined to be 20.1 ± 1.3 Å.

Figure 9 shows the change in oxide thickness, $\Delta d_{ox}$ (the difference between the oxide thickness after anodization and the thickness formed at the OCP), as a function of applied potential in borate buffer pH 7.2. Also shown in this figure is the corresponding total oxide thickness $d_{ox}$ as a function of applied potential. It may be noted that deviations in the thickness of oxide layer formed at the OCP account for the measured "scatter" in the total oxide thickness curve. At applied potentials less than 3 V vs OCP, $\Delta d_{ox}$ increased linearly with applied potential. The oxide growth rate ($\Delta(\Delta d_{ox})/\Delta V_{applied}$) in this region was found to be 6.4 Å/V. Above 3 V vs OCP the change in thickness is approximately 3.0 Å/V. Above 3V, the change in oxide thickness appeared to be less and may have approached a limiting value in total thickness of approximately 55 - 60 Å. In comparison, the anodic film growth rate of aluminum is 13.5 Å/V (24) and grade 2 titanium in 0.1 M HCl is 23 Å/V (21).

Having calculated the oxide thickness, it was possible to make an estimate of the specific oxide resistivity from $R_{ox}$ (see Table 2):

$$\rho_{ox} = R_{ox}A / d_{ox} \tag{3}$$

where $\rho_{ox}$ is the resistivity of the oxide in ohm-cm. Values of $\rho_{ox}$ are presented in Figure 10 as a function of applied potential for the pH 7 solution. Generally, values of $R_{ox}$ were on the order of $10^{10}$ ohm-cm, which agrees well with values reported in literature (25) and is associated more with insulators than semiconductors. As seen in Figure 10, an abrupt decrease in oxide resistivity was observed at approximately 2.1 V vs OCP (approximately +0.72 V SCE). Moreover, the slopes above and below this potential are greatly different. Recall that an abrupt increase in the passive current density was observed in the potential region of approximately 0.60 - 0.83 V vs. SCE during anodic polarization in this solution. From these results we conclude that the increased dissolution rate observed in the potentiodynamic polarization experiments owes to a decrease in the specific resistivity of the oxide. This change may be due to a decrease in the geometric resistivity of the oxide (for example, a transition from compact film to porous film) which allows more easily the transport on ions through the film thus the observed increase in passive current density. It is more likely that the change in oxide resistivity owes to an increase in the concentration of donor species (holes) in the passive film. In addition, as the change in oxide resistivity is clearly reversible (Figure 6) and the EIS measurements were made at the OCP after anodization the relatively small change in oxide resistivity is not unexpected. The observation of oxygen evolution at high applied anodic potentials (Figure 6) is consistent with a more conducting film independent of the mechanism by which the resistivity is decreased.

A decrease in oxide resistivity might also explain the observed change in the relationship between oxide thickness and applied potential from approximately 6.0 Å/V below 3 V vs OCP to approximately 3.0 Å/V above 3 V vs OCP. It has been shown that the ionic current associated with oxide film growth is proportional to the electric field strength in the film(26).

*Breakdown of Passivity in Chloride* Figure 11 shows potentiodynamic polarization curves for S200D beryllium in deaerated NaCl solutions ranging in concentration from $10^{-4}$ to 1 M $Cl^-$. For $Cl^-$ concentrations below 1 M, anodic polarization of the sample was characterized by a region of passivity followed by a logarithmic increase in the current density which corresponded to the onset of pitting corrosion. In deaerated 1 M $Cl^-$, pitting at the OCP was observed. A typical scanning electron micrograph of the corrosion pits found in S200D beryllium following a polarization experiment in 0.01 M NaCl solution is presented in Figure 12. This micrograph is also representative of the corrosion pits found after pitting at the OCP. As seen in this figure, the corrosion pits in Be have the same size and shape as the Be grain morphology. Moreover, the pits are not hemispherical and parallel plates of unattacked Be could be found inside the pits. This type of attack is indicative of etch pits(26). Etch pits are characterized by the formation of specifically shaped cavities in a material that can be related to crystallographic orientation, defect concentration (such as dislocations and vacancies) and the solution to which the material has been exposed. Often the walls which form the etch pit are composed of simple low index crystallographic facets. For example: the pit walls of the polyhedral etch pits created when iron is exposed to methyl alcohol and iodine are formed entirely of {110} facets (28). Similar behavior has been observed in nickel and cobalt (29) as well as in aluminum and stainless steel (30). The orientation of the parallel plates of unattacked Be found inside of the corrosion pits is currently being investigated with Orientation Imaging Microscopy (OIM). OIM allows for the orientation of specific grains in a polycrystalline material to be determined. From knowledge of the local grain character prior to pitting, it should be possible to quantify the orientation of these unattacked parallel plates. In addition we are also investigating the probability of pit initiation as a function of grain orientation for specific grains in polycrystalline Be with this technique. Results of this work will be reported in future publications.

The voltage which corresponded to the onset of pitting corrosion, $E_{pit}$, was found to decrease logarithmically with increasing chloride concentration according to the relationship:

$$E_{pit} = -0.067\log[Cl^-] - 1.01 \tag{4}$$

where $E_{pit}$ is in volts vs. SCE and $[Cl^-]$ is the concentration of chloride in Molarity (Figure 13). As seen in this relationship, a -0.067V change in the pitting potential per decade of chloride concentration was observed. A similar relationship between $E_{pit}$ and chloride concentration has been noted for pure aluminum (Al), however the pitting potential of Al has been found to vary by -0.091V/decade $[Cl^-]$ (31-34). For 18 Cr-8 Ni stainless steel, the pitting potential has been found to vary by -0.088V/decade $[Cl^-]$ (35). Thus, the pitting potentials of Al and stainless steel are more sensitive to changes in chloride concentration than those of Be. In addition, as defined by the y-intercept in Equation 4, for any one chloride concentration $E_{pit}$ for Be is more negative than those of Al and stainless steel. Pitting potentials of historic grades of Be with substantially higher impurity concentrations are currently under investigation. Initial results from that work(36) indicate similar passivity and breakdown behavior as found in S200D Be in this study.

The combined effects of solution pH and chloride concentration on pitting potential are presented in Figure 14. Although the total change in potential over the pH range from 2 to 12.5

was less than 40 mV, a linear relationship between the pitting potential of beryllium when plotted as a function of solution pH was found:

$$E_{pit} = 0.003\text{pH} - 0.96 \qquad (5)$$

This relationship is only valid over the pH range of 2-12.5. Recall that below pH 2, beryllium actively corrodes independent of $Cl^-$ concentration. As indicated by equation 4, the pitting potential is essentially independent of solution pH. Only a slight positive shift was observed in the pitting potential for more alkaline solutions. This same behavior was noted by Leckie and Uhlig for 18Cr-8Ni stainless steel in 0.1 N NaCl solution (36), and others (34).

A somewhat more reproducible parameter for accessing susceptibility to localized attack is the repassivation potential, $E_{repass}$. For beryllium, $E_{repass}$ is plotted as a function of chloride concentration in Figure 15. As the chloride concentration decreases, the potential at which pits repassivate becomes more noble. This trend is characterized by the relationship:

$$E_{repass} = -0.055\log[Cl^-] - 1.06 \qquad (6)$$

where $E_{repass}$ is in volts. This relationship is similar to that observed for $E_{pit}$ where the slope was equal to -0.067 and the intercept equal to -1.01.

*Breakdown of Passivity in Fluoride* Figure 16 shows potentiodynamic polarization curves for beryllium exposed to solutions containing NaF ranging in concentration from $10^{-1}$-$10^{-4}$ M $F^-$. At a $F^-$ concentration of $10^{-4}$ M, anodic polarization of the sample was characterized by a region of passivity followed by a logarithmic increase in the current density which corresponded to the onset of pitting corrosion. The pitting potential was found to be -0.742 V SCE. In comparison, for $10^{-4}$ M $Cl^-$, the pitting potential was -0.773 V SCE. Pitting type corrosion was also observed for $10^{-3}$ M $F^-$, however, no region of passivity was observed upon anodic polarization. A typical micrograph of a Be surface which has suffered pitting attack in $F^-$ solution is presented in Figure 17a. While at the lower fluoride concentrations the breakdown of passivity was localized, at the higher fluoride concentrations ($10^{-1}$ M-$10^{-2}$ M) beryllium was susceptible to uniform attack. A micrograph depicting a typical Be surface after exposure to 0.1M NaF is presented in the optical micrograph in Figure 17b. Although Sheth et al. found that at first glance it appeared that beryllium pits when exposed to 0.1 M KF + $K_2SO_4$ (37), upon polishing below the corrosion product it was discovered that the beryllium had been damaged in a manner consistent with uniform attack. EMF and conductivity measurements have found that a complex film is formed on beryllium when exposed to fluoride (38). Moreover, it was found that the bond between beryllium and fluoride is primarily ionic while the bond between beryllium and other halides is largely covalent. The formation of a fluoride salt film on the surface may explain the observed uniform attack at high $F^-$ concentrations described above.

The combined effects of chloride and fluoride are shown in Figure 18. Addition of low concentrations of NaF to 0.01 M NaCl solutions resulted in an increase of the passive current density, but did not effect the $Cl^-$ pitting potential of the beryllium. Pitting of the beryllium was noted in all solutions containing both fluoride and chloride. Moreover, in solutions which contained both chloride and fluoride, where the concentration of fluoride was high enough to promote uniform attack, localized corrosion rather than uniform attack was observed.

## Summary

The passivity and breakdown of beryllium has been studied using both dc and ac methods. Beryllium has been found to be passive in the pH range from 2-12.5, but is susceptible to uniform attack below a pH of 2. A minimum in both the passive and corrosion current densities was noted in the pH range of 4-11. In solutions containing halides, such as $F^-$ and $Cl^-$, Be was found to be susceptible to pitting corrosion. However, fluoride concentrations above $10^{-2}$ M did not result in pitting attack but rather in uniform attack over the entire Be surface. The pitting potential of beryllium in chloride environments was not found to change substantially with pH. In solutions containing both fluoride and chloride ions, the presence of the fluoride increased the passive current density of beryllium and decreased the pitting potential.

## Acknowledgments

Work on this project was performed under the auspices of the University of California for the United States Department of Energy contract W7405-ENG36. The authors acknowledge the continued support of Doug Kautz and the Surveillance Project Office. The authors would also like to thank Pallas Papin, Bob Reiswig, and JoAnn Montoya for sample preparation and microscopy, as well as George Carlson, Brett Kniss, Gary Devine (LLNL), Jim Oldani (LLNL), and Bill Moddemann (Pantex) for helpful discussions.

## References

1. L.B. Norwood, *SAMPE Journal*, no. 3, 7 (1986).

2. J.M. Finn, Tech. Report AFFDL-TR-67-686 (1967).

3. R.C. Fullerton-Batten and J. A. Hawk, “A Review of Present and Future Applications of Beryllium,” Metals Society Conference Proceedings, Beryllium 1977, London England.

4. M.A. Hill, B.K. Damkroger, R.A. Dixon, E. Robertson, "Beryllium Weldability" in *Weldability of Metals*, R.A. Patterson, K.W. Mahin eds., ASM, Materials Park, 331, (1990).

5. R.D. Watson and J. B. Whitley, *Nuclear Engineering and Design*, Fusion, no. 4, 49 (1986).

6. J.L. English, “Interim Report on the Corrosion of Beryllium in Simulated Cooling Water for the Proposed Development Reactor”, ORNL-298, Oak Ridge National Laboratory, March, 1949.

7. A.J. Stonehouse, W.W. Beaver, “Corrosion and Protection of Beryllium Metal”, BBC-TR 335, The Brush Beryllium Co., December, 1963.

8. D.J. Levy, “The Electrolytic Polarization of Beryllium”, LMSC-6-90-61-75, Lockheed Missiles and Space Division, Sunnyvale, Ca, November, 1961.

9. P.D. Miller, W.K. Boyd, “Corrosion of Beryllium”, DMIC Report 242, Defense Metals Information Center, Battelle Memorial Institute, Columbus, December, 1961.

10. J. J. Mueller and D.R. Adolphson, in *Beryllium Science and Technology*, **2** (ed. D. R. Floyd and J. N. Lowe), Plenum Press, New York, 417 (1979).

11. E. Gulbrandsen and A. M. J. Johansen, *Corrosion Science*, **36**, 1523 (1994).

12. M.A. Hill, D.P. Butt, R.S. Lillard, "The Corrosion/Electrochemistry of Beryllium and Beryllium Weldnments in Aqueous Chloride Environments", LAUR-96-3669, Los Alamos National Laboratory, Los Alamos, NM, October (1996).

13. R.S. Lillard, M.A. Hill, D.P. Butt, "Preliminary Investigation into the Corrosion of Beryllium Exposed to Celotex and Water", LAUR-97-0854, Los Alamos National Laboratory, Los Alamos, NM, February (1997).

14. M.A. Hill, D.P. Butt, R.S. Lillard, "The Passivity and Breakdown of Beryllium in Aqueous Solutions", LAUR-97-5007, Los Alamos National Laboratory, Los Alamos, NM, November (1997).

15. A. James Stonehouse, *J. Vac. Sci. Technology A*, **4**, 1163 (1986).

16. M.E. Straumanis and D.L. Mathis, *J. Electrochem. Soc.*, **109**, 434 (1962).

17. M. Pourbaix, *Atlas of Electrochemical Equilibria in Aqueous Solutions*, Pergammon Press, New York, 135 (1966).

18. D. Landolt, in *The Passsivity of Metals*, R.P. Frankenthal and J. Kruger eds., p. 484, The Electrochemical Society, Princeton (1978).

19. Metals Handbook, vol. 13, ASM International, Metals Park, Ohio, 66 (1987).

20. K. Azumi, T. Ohtsuka, N. Sato, *J. Electrochem. Soc.*, **134**, 1352 (1987).

21. D.G. Kolman and J.R. Scully, *J. Electrochem. Soc.,* **140**, 2771 (1993).

22. A. E. Bohe, J. R. Vilche, K. Juttner, W. J. Lorenz, W. Kautek, and W. Paatsch, *Corrosion Science,* **32**, 621 (1991).

23. R. F. Geller, R. I. Yavorsky, B. L. Steierman, and A. S. Creamer, *Journal of the National Bureau of Standards,* **36**, 277 (1946).

24. K. Videm, *The Electrochemistry of Uniform Corrosion and Pitting of Aluminum,* Institutt for Atomenergi, Kjeller, Norway (1974).

25. H. H. Coobs and W. J. Coshuba, *J. Electrochem. Soc.,* **99**, 115 (1952).

26. D.A. Vermilyea, "Anodic Oxides", in: *Advances in Electrochemistry and Electrochemical Engineering, vol. 3, Electrochemistry,* Interscience, New York, 1963.

27. M.B. Ives, “Etch Pitting - Theory and Observation”, in *Localized Corrosion,* R.W. Staehle, B.F. Brown, J. Kruger, A. Argrawal eds., NACE, Houston, 78, (1986).

28. J.P. Kauffman, J. Bardolle, *Compt. Rend.*, (Paris), vol. 266C, pp. 439, 1968.

29. J.P. Kauffman, J. Bardolle, *Compt. Rend.*, (Paris), vol. 270C, pp. 165, 1970.

30. S. Szklarska-Smialowska, “The Pitting of Iron-Chrome-Nickel Alloys”, in *Localized Corrosion*, R.W. Staehle, B.F. Brown, J. Kruger, A. Argrawal eds., NACE, Houston, 312, (1986).

31. S. T. Pride, J. R. Scully, and J. L. Hudson, *J. Electrochem. Soc.*, **141**, 3028 (1994).

32. J. R. Galvele and S. M. De Micheli, *Corrosion Science,* **10**, 795 (1970).

33. Z. A. Foroulis and M. J. Thubrikar, *Electrochemica Acta,* **21**, 225 (1976).

34. Z. Szlarska-Smialowska, *Pitting Corrosion of Metals,* NACE, Houston, Texas 221 (1986).

35. H. P. Leckie and H. H. Uhlig, *J. Electrochem. Soc*., **113**, 1262 (1966).

36. D,K, Kolman, unpublished data, 1997.

37. K. G. Sheth, J. W. Johnson, and W. J. James, *Corrosion Science,* **9**, 135 (1969).

38. D. A. Everest, *The Chemistry of Beryllium*, Elsevier, 38 (1964).

# Tables

**Table 1**. Typical Be S200D and Be S200F chemistries. All values are given in weight percent.

| Constituents | S200F | S200D |
|---|---|---|
| Beryllium | 98.5 | 98.0 |
| Beryllium Oxide (BeO) | 1.5 | 2.0 |
| Aluminum | 0.10 | 0.16 |
| Carbon | 0.15 | 0.15 |
| Iron | 0.13 | 0.18 |
| Magnesium | 0.08 | 0.08 |
| Silicon | 0.06 | 0.08 |
| Other Metallic Impurities | 0.04 | 0.04 |

**Table 2** Parameters from CNLS modeling of EIS data (Figure 7) as a function of anodization potential for Be in pH 7.2, 0.5 M boric acid / 0.05 M sodium borate buffer solution.

| Applied Potential (volts vs OCP) | Charge Transfer Resistance; $R_{ct}$ (ohm-cm$^2$) | Oxide Resistance; $R_{ox}$ (ohm-cm$^2$) | Oxide Capacitance; $C_{ox}$ (µFarads/cm$^2$) |
|---|---|---|---|
| 0.5 | 2.90x10$^{6}$ | 5329 | 2.569 |
| 1.0 | 4.72x10$^{6}$ | 7729 | 2.198 |
| 1.5 | 5.56x10$^{6}$ | 6004 | 1.938 |
| 2.0 | 7.10x10$^{6}$ | 6376 | 1.776 |
| 2.5 | 7.28x10$^{6}$ | 3899 | 1.583 |
| 3.0 | 8.44x10$^{6}$ | 3755 | 1.553 |
| 4.0 | 7.90x10$^{6}$ | 1685 | 1.425 |
| 5.0 | 1.49x10$^{6}$ | 4164 | 1.265 |
| 6.0 | 6.67x10$^{6}$ | 4650 | 1.161 |
| 7.0 | 6.94x10$^{6}$ | 3991 | 1.174 |
| 8.0 | 1.14x10$^{7}$ | 3706 | 0.994 |

## Figures

NOT PRESENTED

Figure 1. Polarized light micrograph of S200D Be. The small (1 µm) dark features are BeO particles, some of which are indicated by arrows. Also note the grain size of approximately 10-40 angstroms and grain structure.

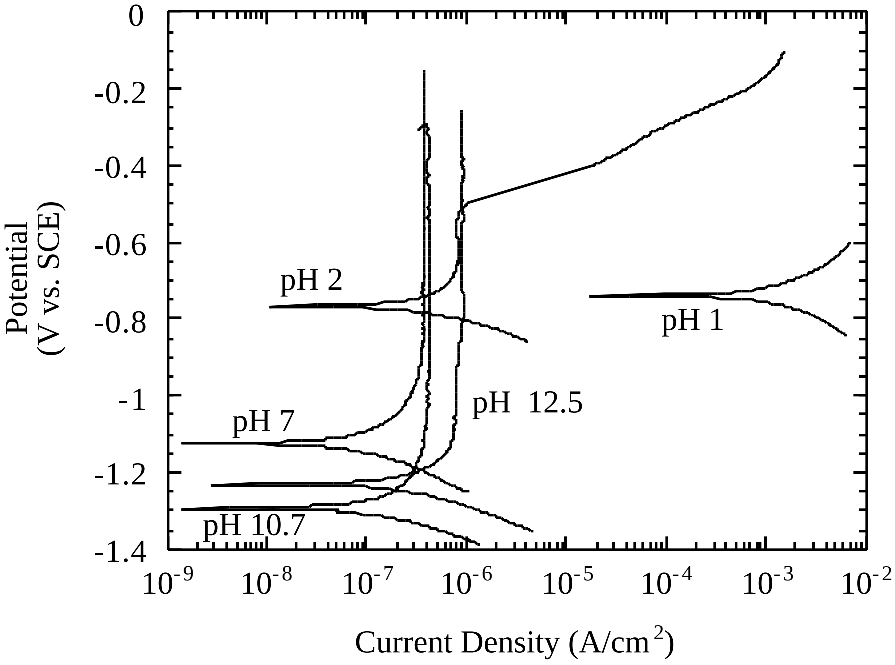

Figure 2. Beryllium polarization curves as a function of solution pH. Between 2 and 12.5 passivity was observed, while below pH 2 Be was susceptible to uniform attack.

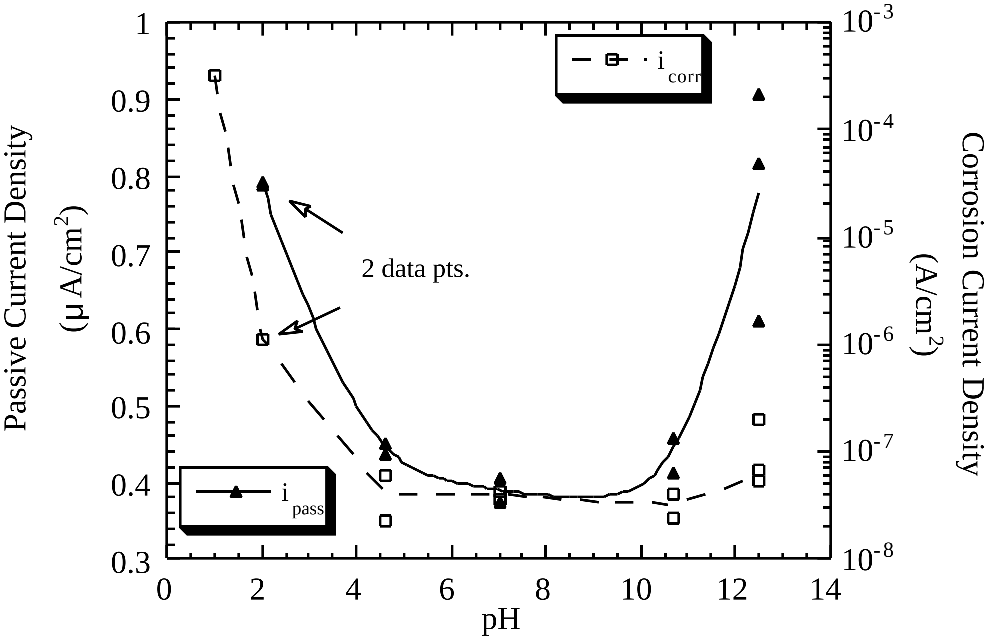

Figure 3. Passive current density, $i_{pass}$, and corrosion current density, $i_{corr}$, as a function of solution pH. A minimum in $i_{pass}$ and $i_{corr}$ exists between a pH of 4.5 and 10.7.

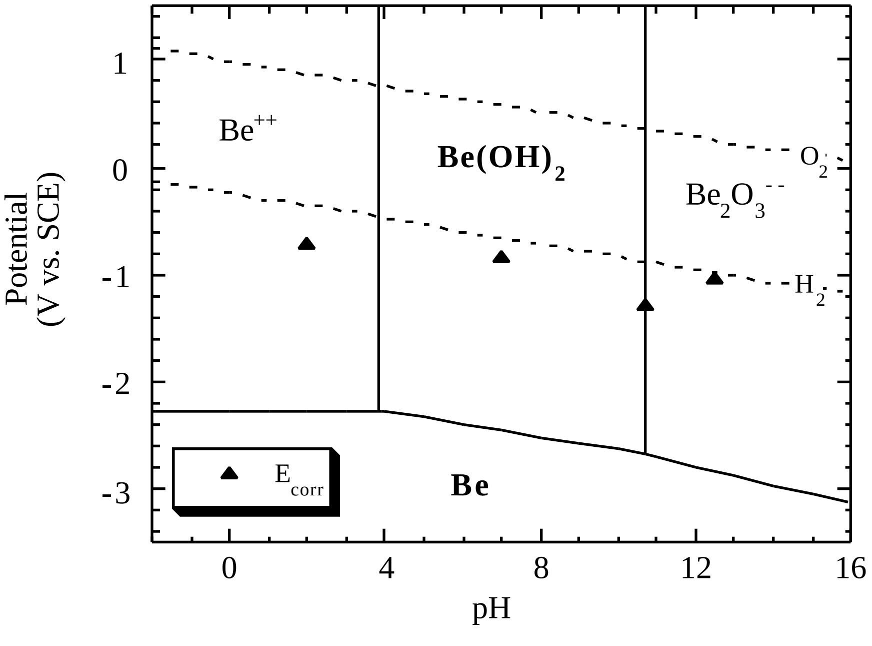

Figure 4. Potential-pH diagram for the Be-water system at 25°C for the $\beta-Be(OH)_2$ crystalline hydroxide and assuming a $10^{-6}$ M concentration of $Be^{++}$.

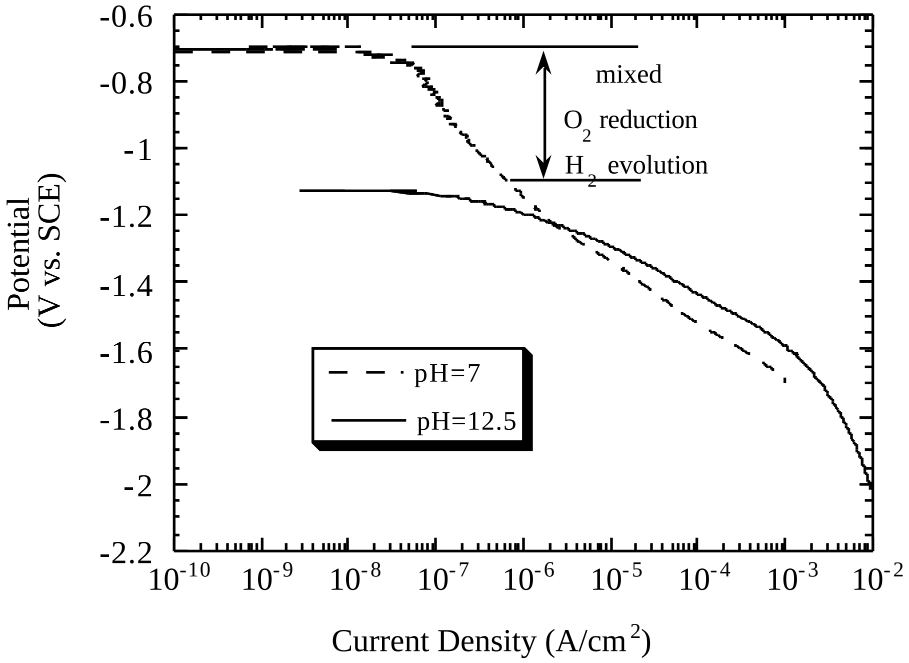

Figure 5. Cathodic polarization curves for Be in pH 7.2 boric acid/ sodium borate buffer solution and pH 12.5 NaOH solution.

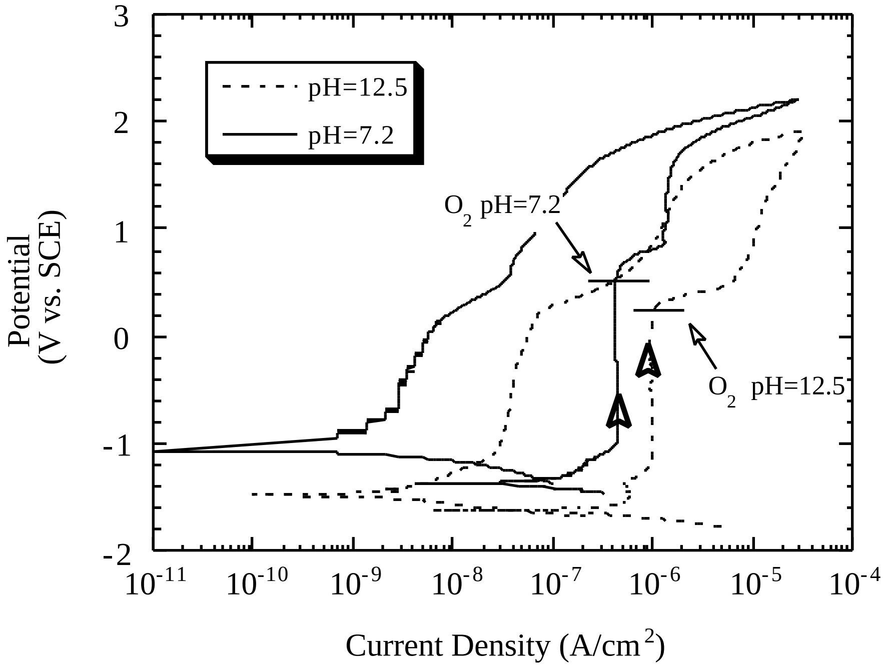

Figure 6. Potentiodynamic polarization curves of beryllium in pH 7.2 boric acid/sodium borate buffer solution and pH 12.5 NaOH solution showing an increase in current density at potentials above 0.6V vs. SCE.

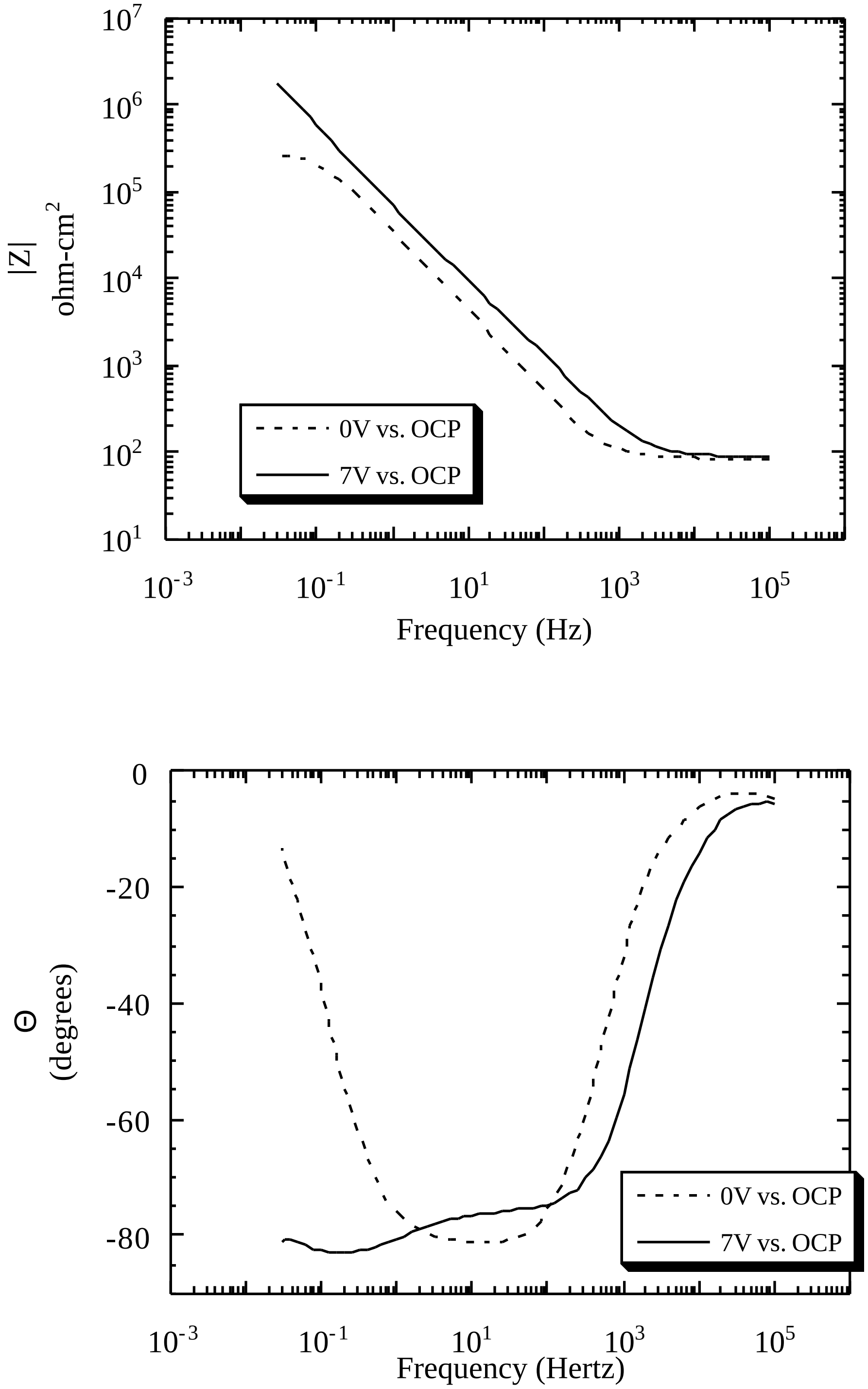

Figure 7. a) Bode magnitude b) Bode phase plots for Be prior to anodization (0V vs. OCP) and following anodization at an applied potential of 7V (pH 7.2 boric acid/ sodium borate buffer anodization solution).

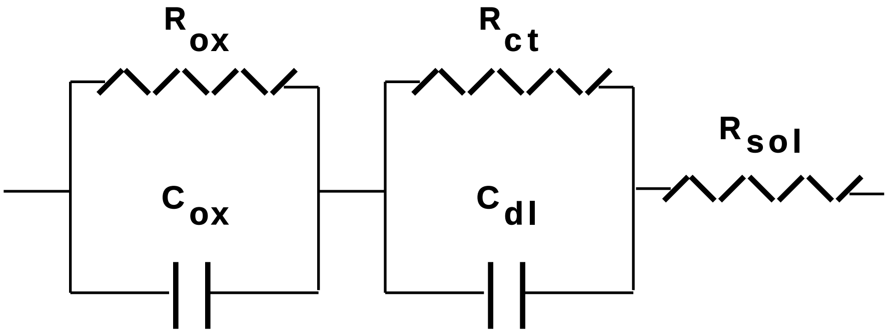

Figure 8. Equivalent circuit used to model a passive Be surface exposed to an aqueous solution.

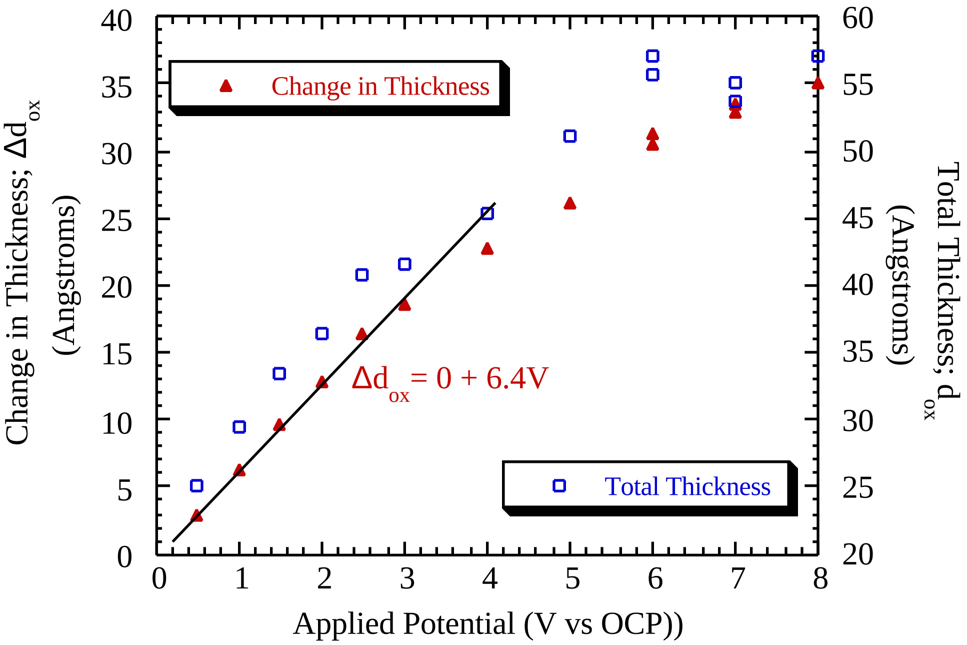

Figure 9. Change in oxide thickness (the difference between the total oxide thickness after anodization and oxide thickness measured at the OCP prior to anodization) and total oxide thickness after anodization as a function of applied potential.

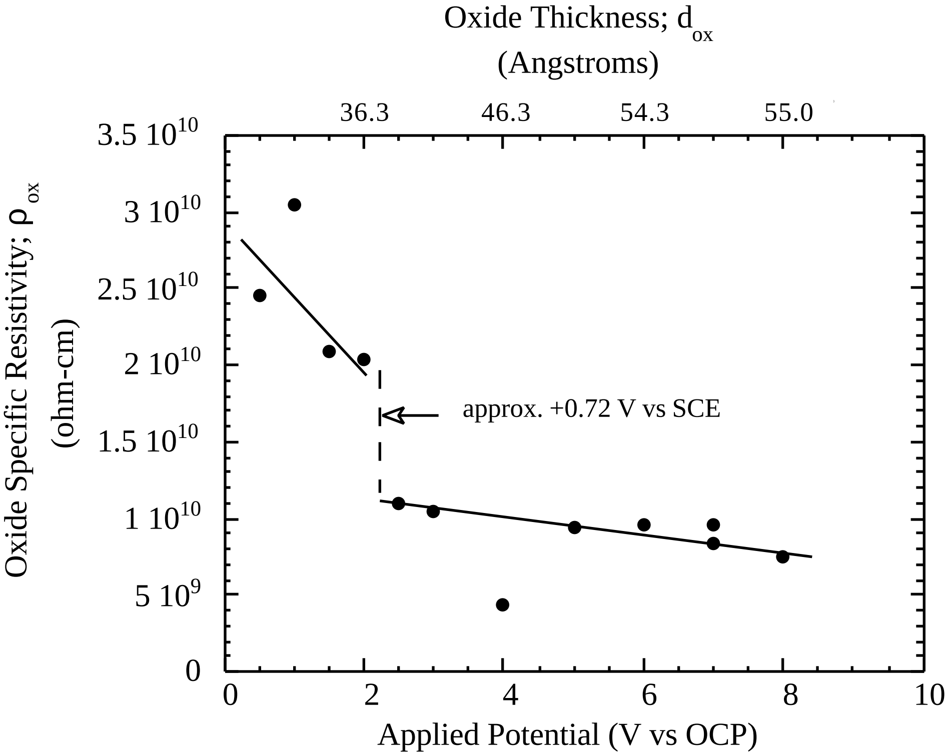

Figure 10. Specific resistivity of the oxide on Be as a function of applied voltage. Values were calculated from the EIS circuit model parameters and the measured oxide thicknesses.

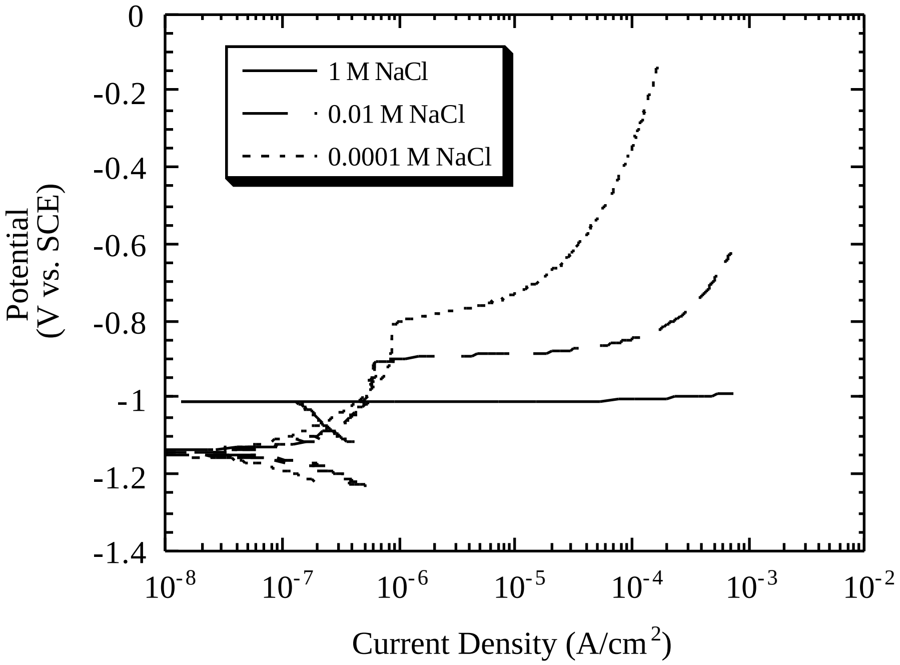

Figure 11. Beryllium polarization curves as a function of chloride concentration showing a decrease in pitting potential with an increase in chloride concentration.

NOT PRESENTED

Figure 12. SEM micrograph of a corrosion pit in S200D Be showing parallel plates of Be left behind after pit propagation ceased. The size of any one set of parallel plates is consistent with the grain size in this material (about 10-40 angstroms).

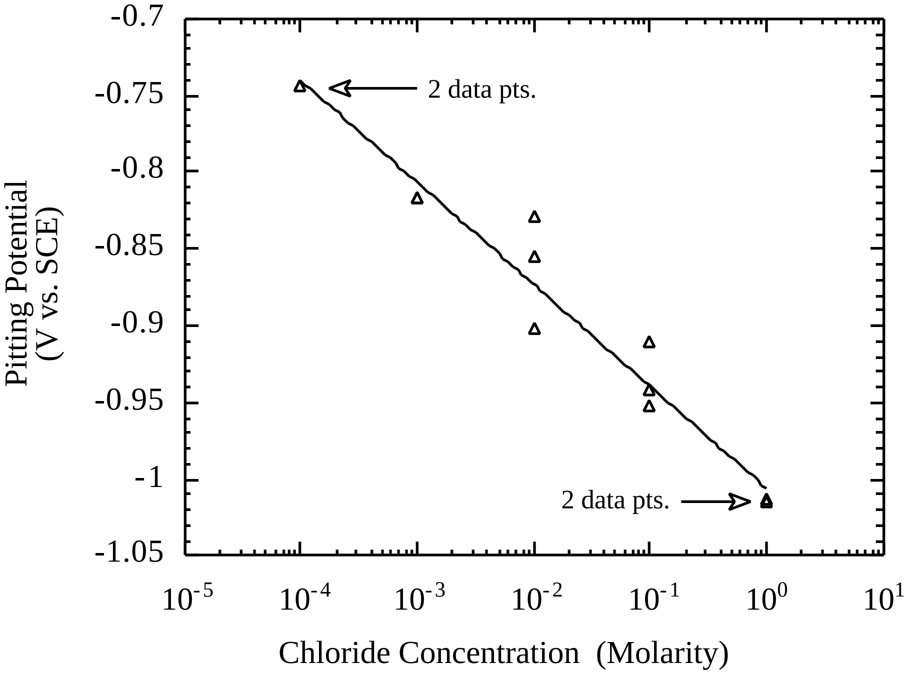

Figure 13. Pitting potential as a function of chloride concentration displaying a logarithmic relationship between $E_{pit}$ and [$Cl^-$].

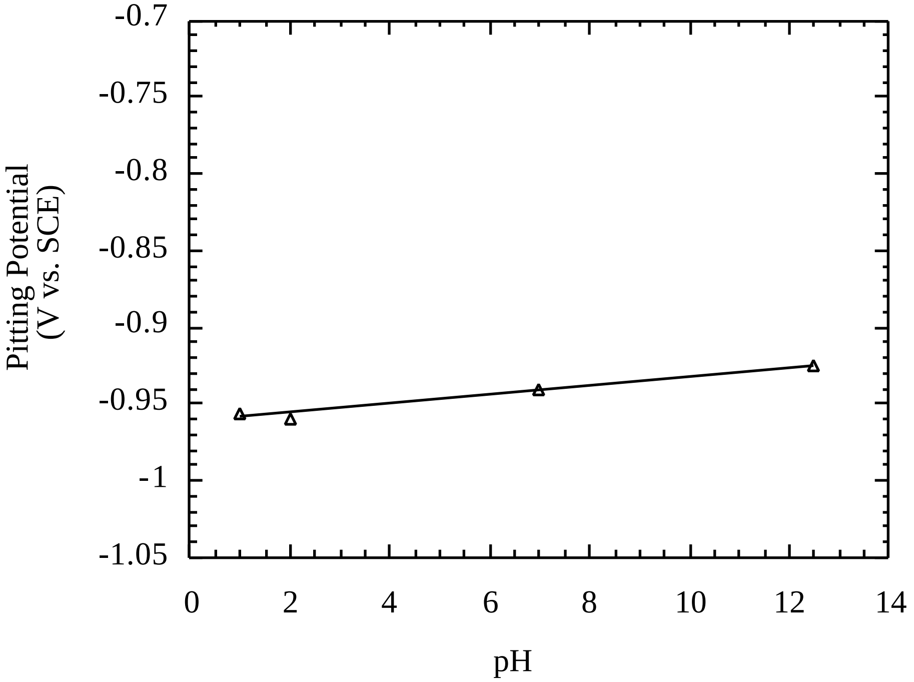

Figure 14. Pitting potential as a function of solution pH in 0.1 M NaCl showing a small linear increase in $E_{pit}$ with increasing solution pH.

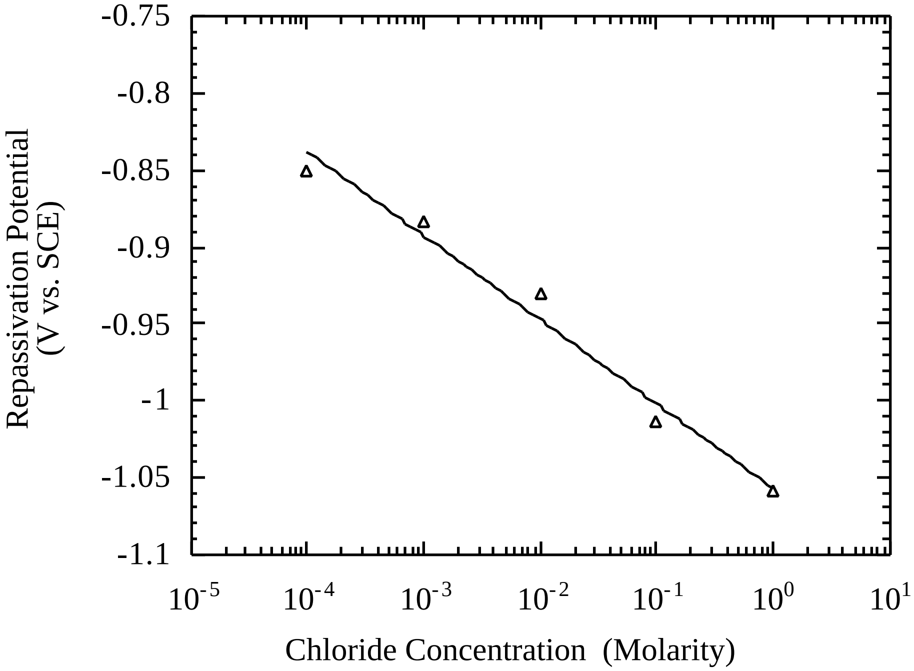

Figure 15. Repassivation potential as a function of chloride concentration showing a logarithmic relationship between an increase in potential with an increase in chloride concentration.

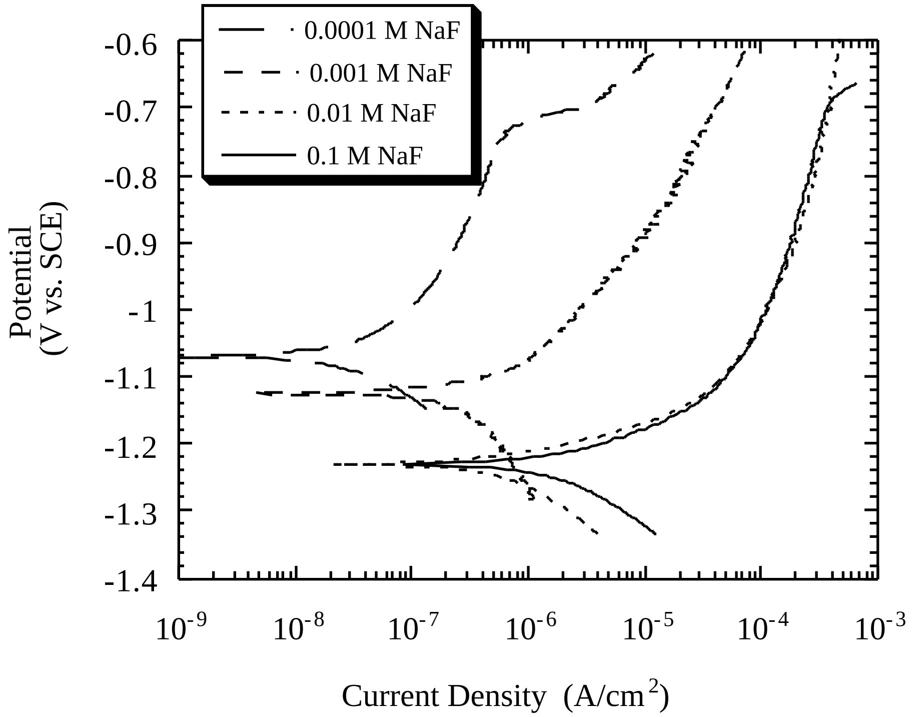

Figure 16. Beryllium polarization curves as a function of fluoride concentration. Beryllium pits at lower concentrations while it anodically dissolves at higher fluoride concentrations.

NOT PRESENTED

Figure 17 Micrographs depicting the 2 types of attack observed on Be in F- solutions: a) bright field micrograph of beryllium after potentiodynamic polarization in 0.001 M NaF showing corrosion pits. b) dark field micrograph of beryllium after potentiodynamic polarization in 0.1 M NaF.

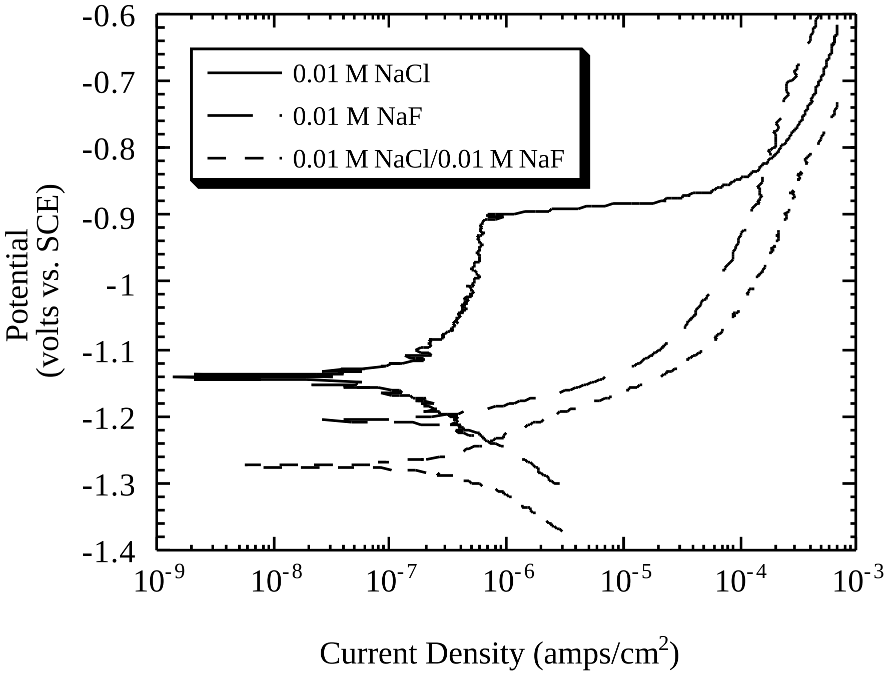

Figure 18. Potentiodynamic polarization curves of beryllium in 0.01 M NaCl, 0.01 M NaF, and 0.01 M NaCl/0.01 M NaF. Pitting of the beryllium occurred in the presence of Cl$^-$. The beryllium anodically dissolved in the NaF at this concentration.